remote sensing

MDPI

Article

Surging Dynamics of Glaciers in the Hunza Valley under an Equilibrium Mass State since 1990

Kunpeng Wu [1,2,*], Shiyin Liu [1,2], Zongli Jiang [3], Yu Zhu [1,2], Fuming Xie [1,2], Yongpeng Gao [1,2], Ying Yi [1,2], Adnan Ahmad Tahir [4] and Saifullah Muhammad [1,5]

1 Institute of International Rivers and Eco-Security, Yunnan University, Kunming 650091, China; shiyin.liu@ynu.edu.cn (S.L.); yuzhu@mail.ynu.edu.cn (Y.Z.); xfm@mail.ynu.edu.cn (F.X.); 22019000220@mail.ynu.edu.cn (Y.G.); yingyi@mail.ynu.edu.cn (Y.Y.); Saif_2146@yahoo.com (S.M.)
2 Yunnan Key Laboratory of International Rivers and Transboundary Eco-Security, Yunnan University, Kunming 650091, China
3 Department of Geography, Hunan University of Science and Technology, Xiangtan 411201, China; jiangzongli@hnust.edu.cn
4 Department of Environmental Sciences, COMSATS University Islamabad, Abbottabad Campus, Abbottabad 22060, Pakistan; Adnantahir@cuiatd.edu.pk
5 Department of Agricultural Engineering, Muhammad Nawaz Sharif University of Agriculture Multan, Multan 66000, Pakistan
* Correspondence: wukunpeng@ynu.edu.cn

Received: 6 August 2020; Accepted: 7 September 2020; Published: 9 September 2020

Abstract: Previous studies have shown that glacier changes were heterogeneous in the western Karakoram, with the coexistence of retreating, advancing, and surging glaciers. However, it remains unclear that the mechanisms driving these changes. Based on the Shuttle Radar Topography Mission (SRTM) DEM and TerraSAR-X/TanDEM-X images (2014), this study presents glacier surface height changes in the Hunza Basin of the western Karakoram, employing the method of differential synthetic aperture radar interferometry (DInSAR). A slight negative glacier mass balance was observed in the Hunza Basin during 2000–2014. Surge-type glaciers would not have an obvious effect on overall mass balance in regional assessments over long-time scales. Further, glacier surface velocities in the Hunza Basin were estimated from Landsat images for the period of 1990–2018 by utilizing published data sets and Landsat images. Compared to the annual glacier surface velocities, 22 surge events were observed in seven surge-type glaciers in the Hunza Basin. Glacier flow can be attributed to thermally and hydrologically control, and the geomorphological characteristics of different individuals. This study gives us a new insight into the situation of the "Karakoram anomaly" under the background of glacier mass loss in the high mountains of Asia (HMA).

Keywords: glacier surging; mass balance; karakoram anomaly; DInSAR; feature tracking

1. Introduction

Glaciers in the high mountains of Asia (HMA) are the sources of many major rivers and lakes in Asia [1]. As sensitive climate indicators, continuous long-term monitoring on glacier is increasingly important for the interpretation of global changes [2]. Because of global warming in recent decades, the mass loss in the HMA from 2003 to 2009 accounts for ~10% to the global glacier mass loss, which contribute 3% to the sea level rise [3], and debris coverage in glacier increased [4]. Meanwhile, the frequency of glacial hazards increased, such as glacial lake outburst floods (GLOF) and glacier surge [5–7]. Despite in-situ observations being encouraged, the great labor cost and rugged terrain has limited its application in the HMA. Based on geodetic methods, previous studies have shown that glacier mass balance was heterogeneous in the HMA [8–10]. A significant impact can be made by local

parameters on glacier responses to climate change; therefore, there may have a heterogeneous pattern of glacier changes [11].

In contrast to the Nyainqentanglha, Tien Shan, and Himalayas, which were experiencing pronounced negative glacier mass balances [8,12], a complex pattern of glacier changes had been evident for the Karakoram, the Western Kunlun, and the Pamirs in recent decades [2,8,13]. Due to the occurrence of surges and complex glacier behaviors [14], these results of mass gain are difficult to interpret. Furthermore, many glaciers in the western Karakoram are covered by debris [13]. Influenced by supraglacial debris, glacier termini can reach to lower elevations and react differently to warming [13,15]. However, it remains unclear whether the debris cover has any impact on glacier surges or other complex behaviors. Hence, the details of the "Karakoram anomaly" remain controversial and deserves more attention.

Glacier surface height changes and velocities are particularly crucial parameters that determine glacier discharge. Measurements of these parameters could help us to better understand the glacier responses to climate change [16,17]. Predecessors in glacier surface height changes and velocities in western Karakoram have already done a lot of significant research work and achieved fruitful results [8–10,13,18–21], and the relation between the two crucial parameters is fairly precise [22]. For complex patterns of glacier changes in western Karakoram, several mechanisms are proposed, while there are knowledge gaps and uncertainty [22]. In our study, the decadal glacier mass balance in the Hunza Basin of the western Karakoram was estimated from the differential synthetic aperture radar interferometry (DInSAR) method on the Shuttle Radar Topography Mission (SRTM) DEM and TerraSAR-X/TanDEM-X (TSX/TDX) images (2014). Additionally, glacier surface velocities in the Hunza Basin were derived from Landsat images for the period of 1990–2013 by utilizing cross-correlation feature tracking techniques. Based on the analysis of mass balance and annual variability of velocity, the spatiotemporal variabilities of glacier were investigated in the western Karakoram.

2. Study Area

The Hunza Basin (35°42′–37°06′ N, 72°30′–75°47′ E), located in the western Karakoram, is one of the glaciated sub-catchment of the Upper Indus Basin (Figure 1). The typical characteristics of the study area are steep valley walls and narrow valleys [23]. The Hunza River is contributed by more than 14 small and medium sized tributaries, such as Khynjerab, Hispar, Hassanabad, Mulungutti, and Verjerab.

The Hunza Basin, located in subtropical climate zone, is affected by the Westerlies and the Indian Summer Monsoon [24]. Mean annual temperature ranges from 2.8 to 6.5 °C in the valleys at the elevation of 2810–3669 m a.s.l. [24], and mean daily temperature ranges from −9.0 °C in January to 14.6 °C in July based on observations at Ziarat (3669 m a.s.l.) [25]. Due to the limitation of high mountains, the influence of monsoon weakens north-westward [26]. While the Westerlies brings intensity precipitation in both summer and winter, about 2/3 of high-altitude snowfall in the study area result from the Westerlies [27]. The snow cover in winter is about 80% and decreases to 30% in summer [28].

Based on the Randolph Glacier Inventory, 2209 glaciers developed in the Hunza Basin, with glacier area of 4403.5 km^2 [29]. Due to great vertical height difference and abundant precipitation, many large valley glaciers developed in the Hunza Basin. The equilibrium-line altitude (ELA) in study area ranges from 4500 m to 5500 m a.s.l. [9,11,30]. The ablation areas of most glaciers are covered by debris, and about 90% of glacier area lies in the 5000–6000 m elevation range [31]. Using CORONA and Landsat imagery, glacier area in the Hunza Basin decreased by 1.36% from 1973–2014 [24]. Many glaciers surged in recent years, such as Hispar Glacier, Khurdopin Glacier, and Shishper Glacier [14,32,33].

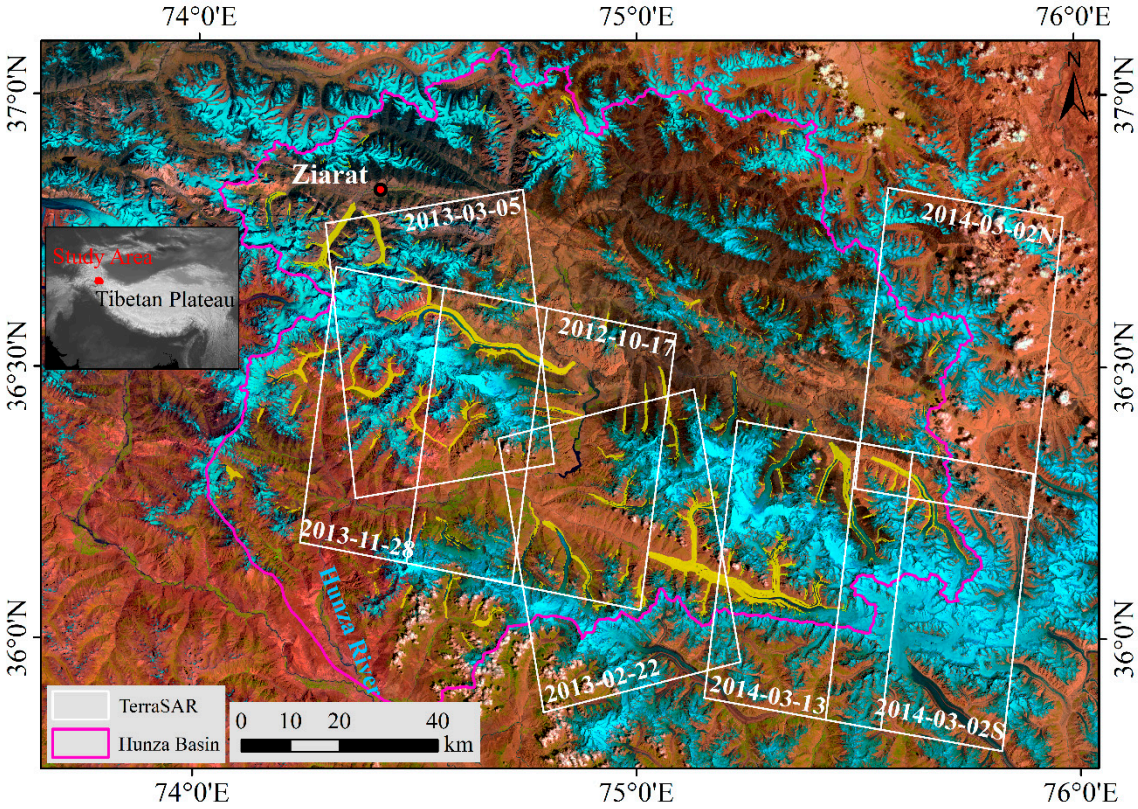

Figure 1. Regional overview of the study area in the Hunza Basin, western Karakoram. Background: Landsat Operational Land Imager (OLI) image (Bands 6, 5, and 3) mosaicked from LC81490342013202LGN00, LC81490352013202LGN00, LC81500342014260LGN01, and LC81500352013209LGN00. Light blue areas represent bare ice, red-brown areas represent bare soil and rocks, green areas represent grass or other vegetation, and yellow areas represent debris-covered glaciers.

3. Methods

3.1. Glacier Outlines

Glacier outlines could be acquired from the Randolph Glacier Inventory [29]. For the Hunza Basin, these glacier outlines acquired from Landsat images during the period 1998 – 2002. To analyze the changes of surface elevation and velocities, glacier extents in different periods should be considered, especially in the Karakoram region, where more than 50% of glaciers advanced. Hence, glacier mapping in 2014 was delineated in this study.

A semi-automated approach was employed to acquire glacier outlines in 2014 from Landsat OLI images. This approach was applied at the cloud-computing platform Google Earth Engine (GEE) [34]. First, a pixel-based approach was used to select the suitable images [34]. To minimize the effect of snow cover, all images during January 2013–December 2015 were selected from the ablation season from July to October. Using a cloud score algorithm, pixels of cloud cover in the images were masked [35]. Next, to filter the remaining clouds and shadows, the 30th to 70th percentile range of the entire image stack were used to calculate a mean value for each pixel [34]. Then, ice/snow body was identified from resulting image by the normalized difference snow index (NDSI) [36]. The NDSI $[(\lambda_{green} - \lambda_{SWIR1})/(\lambda_{green} + \lambda_{SWIR1})]$ includes Landsat OLI band 3 (green) and band 6 (SWIR1). Based on the NDSI image and threshold value, ice/snow body was distinguished from other land cover types. For isolated ice/snow patches smaller than 0.01 km^2, they were eliminated by a 3 × 3 median filter [37].

Finally, to discriminate clean ice and seasonal snow, the derived glacier outlines were checked manually. The distribution of debris cover is an important parameter in the western Karakoram; therefore, the same method (NDSI from Landsat images in the GEE platform) but different threshold value (NDSI < 0.4) were used to derive debris-covered ice surfaces.

Comparing delineated outlines with ground truth or reference data derived from high-resolution air photos is a good way to assess the uncertainty of glacier mapping [38]. A previous study indicated that the average offsets of glacier outlines acquired from Landsat image were ±10 m for clean ice and ±30 m for debris-covered areas, respectively [39]. Based on these results, an uncertainty of ±4.6% were calculated for glacier outlines in 2014.

3.2. Glacier Height Changes

Glacier height changes (ΔH) were calculated from seven TSX/TDX acquisitions and the SRTM DEM. The SRTM C-band DEM with one arc second resolution in WGS84/EGM96 was used in this study. Flying in close orbit formation, the TerraSAR-X and TanDEM-X act as a flexible single-pass SAR interferometer [40]. Acquired in bistatic InSAR stripmap mode, seven pairs of X-band bistatic TSX/TDX acquisitions were used to derive glacier height change (Figure 1, Tables 1 and 2). In the ground range and azimuth direction, the resolutions of TSX/TDX image were both ~2.5 m.

Table 1. Overview of satellite images and data sources.

Acquisition Date	Mission	Path/Row	Pixel Size (m)	Application
11–22 February 2000	SRTM C-band	-	30	Estimation of glacier elevation change
24 July 2014	Landsat OLI	149/35	15	Glacier identification for 2014
17 October 2012 22 February 2013 5 March 2013 28 November 2013 2 March 2014N 2 March 2014S 13 March 2014	TSX/TDX	-	12	Estimation of glacier elevation change
March 2013–December 2018	Landsat OLI	149/35	15	Estimation of glacier surface velocity

Table 2. Specification of the bistatic TSX/TDX SAR dataset used.

Acquisition Date	Orbit	Orbital Pass	Effective Perpendicular Baseline (m)	Master Satellite
28 November 2013	113	Descending	161	TSX
17 October 2012	113	Descending	151	TSX
5 March 2013	7	Ascending	110	TSX
22 February 2013	7	Ascending	117	TSX
13 March 2014	151	Descending	155	TSX
2 March 2014N	151	Descending	143	TDX
2 March 2014S	151	Descending	143	TDX

Based on the method of DInSAR, the TSX/TDX acquisitions were processed by interferometric processing software [12]. Glacier height changes can be acquired from bistatic interferograms, while topographic phases and flat earth, contained in bistatic interferograms, should be removed first. The flat earth and topographic phases were simulated by orbital information from SRTM DEM and TSX/TDX acquisitions, and then removed from the bistatic interferogram and leave the topographic residual phase, which called differential interferogram. The topographic residual phase, mainly caused by the change of glacier height, can be converted to height changes directly [41–43].

Using an intensity cross-correlation algorithm, a refinement of the lookup table was acquired from a horizontal co-registration between the SRTM DEM and the TSX/TDX acquisition [44]. The refinement of the lookup table and precise orbit information of the TSX/TDX scene were used to eliminate the horizontal offsets between the TSX/TDX acquisition and SRTM DEM. Using GAMMA's minimum cost flow algorithm, differential interferogram was unwrapped and converted to absolute differential heights [45].

Because of the poor quality of coherence for topographic measurement, foreshortening, layover, and shadow regions of the TSX/TDX interferogram cannot be used. The unusable regions were masked out. Assuming that elevation changes is similar at the same altitude [9], the changes of glacier height were calculated in each 100 m altitude bands [46], and "no data" pixels were replaced with the mean ΔH of the corresponding altitude band [47].

The penetration depth of microwaves into the snow, firn, and ice can range from 0 m to 10 m [48]. Hence, glacier surface elevation derived from InSAR might be lower than the actual glacier surface. Due to the advantage of high resolution, large coverage, and freely availability, the SRTM DEMs are being used in many studies; therefore, the penetration depth of SRTM is widely discussed [9,10,12,41,46]. The published value from Lin et al. [46]—a penetration depth of 2.41 ± 0.17 m for the Karakoram region—was applied in this study. Considered that the observed time of TSX/TDX were closed to the performed time of SRTM, and the carrier frequencies of the SRTM X-band and TSX/TDX are almost the same, Lin et al. [46] presumed that no penetration difference exists between the SRTM X-band DEM and TSX/TDX. Hence, the elevation difference between SRTM X-band and C-band DEM can be regarded as the penetration depth when the changes of glacier height calculated from TSX/TDX and SRTM C-band DEM.

The changes of glacier height were converted into mass balance by the ice/firn/snow density of 850 ± 60 kg/m^3 [49]. Assuming that heights remains unchanged in non-glacier areas for a long time, the mean elevation differences (MED) and standard deviation (SD) in non-glacier areas can be used to estimate the errors of the changes of glacier heights. In order to reduce the error of autocorrelation, a distance of 500 m was chosen for difference map derived from SRTM DEM and TSX/TDX. Hence, the overall errors of the changes of glacier height can be calculated by

$$\sigma = \sqrt{\mathrm{MED}^2 + \left(\frac{\mathrm{SD}}{\sqrt{N}}\right)^2} \quad (1)$$

where N is the pixel number with effective measurements. Overall, the error of mass balance was calculated by the errors of glacier area, height changes, and ice density uncertainty.

3.3. Glacier Surface Velocities

Based on the auto-RIFT feature tracking, the Inter-Mission Time Series of Land Ice Velocity and Elevation (ITS_LIVE) project extracted annual mean surface velocities for major glacier-covered regions from Landsat imageries [50,51]. Due to the low quality of data sources, the ITS_LIVE data product has large uncertainty in the earlier product years. Therefore, glacier surface velocities in the Hunza Basin from 1990–2018 were used in this study.

In addition, seasonal surface velocities in the period of 2013–2019 were estimated from Landsat OLI images using cross-correlation feature tracking techniques. This application was processed on Co-Registration of Optically Sensed Images and Correlation (COSI-Corr), an IDL module for the remote sensing platform ENVI [52]. Previous studies have proved that cross-correlation feature tracking on COSI-Corr is an effective method for measuring glacier surface velocity [53–55].

First, the 15-m panchromatic band of the Landsat OLI images was co-registered to a common reference dataset. Then, horizontal ground displacements were estimated from sub-pixel correlation of co-registered images. With search windows of 64 × 64 pixels (pattern size) and 128 × 128 pixels (search area), image correlation was acquired iteratively [20,55]. The east–west and north–south displacements and signal-to-noise ratio (SNR) were yielded by image correlation. Glacier velocity were obtained by the combination of horizontal ground displacements. In order to improve the accuracy of surface displacement, image matches that SNR < 0.9 and extreme values were removed [20]. Finally, the surface displacement converts into annual glacier surface velocity by using the following equation:

$$GSV = \frac{GSD}{T_i} \times T_y \quad (2)$$

where GSV is the glacier surface velocity, GSD is the glacier surface displacement, T_i is the time interval, and T_y is a constant of 365 or 366.

As with the glacier height changes, the uncertainties of glacier velocity were estimated by the residual value in non-glacier areas. Gaussian low path filtering was used to smooth the velocity map in order to minimize the effect of autocorrelation [54]. Thus, image pairs separated by ~365 days were used to measure annual glacier surface velocity. The uncertainties of annual and seasonal glacier surface velocity depend on the time separation between the images, ranging from 2–20 m a^{-1} and 0.02–1.00 m d^{-1}, respectively.

4. Results

4.1. Mass Balance

The average surface thinning of glacier in the Hunza Basin was −0.61 ± 0.07 m from 2000 to 2014 (Figure 2a and Table 3). Glaciers with an area of 2878.2 km^2 experienced a mean mass balance of −0.04 ± 0.02 m w.e. a^{-1}. Overall, mass balance increased with altitude, and it varied significantly in different elevation ranges (Figure 3). Glaciers experienced a negative mass balance of −0.21 ± 0.02 m w.e. a^{-1} below 5100 m a.s.l., while it turned to a positive mass balance of 0.11 ± 0.02 m w.e. a^{-1} above 5100 m a.s.l. during 2000–2014. Even though glaciers experienced a negative mass balance below 5100 m a.s.l., a significant thickening was observed in the 3800–4100 m a.s.l.; the main reason for this phenomenon is glacier surging in Hispar Glacier.

The ablation area of many glaciers in the Hunza Basin are covered by debris. The total debris-covered area of 587.8 km^2 account for ~13.3% of the total glacier area. Approximately 98.3% of the debris-cover is found in the 2700–5200 m a.s.l. range. Compared with clean ice in the same elevation range in all non-surging glaciers, negative mass balance was greater on the debris-covered area during 2000–2014 (−0.46 ± 0.15 m w.e. a^{-1} on debris-covered area vs. −0.08 ± 0.02 m w.e. a^{-1} on clean ice). This indicated that the debris cover has an acceleration effect on surface melting overall, whereas the debris cover has different impact in different elevation ranges (Figure 3).

Glaciers in the study area experienced retreating, advancing, surging, or quiescent phases. After surging, heterogeneous mass balance was observed in these glaciers during 2000–2014. According to the classification of surge and non-surge glaciers, surge glaciers experienced a negative mass balance of −0.06 ± 0.02 m w.e. a^{-1}, it was larger than the negative mass balance of non-surg glaciers (−0.03 ± 0.02 m w.e. a^{-1}). All the non-surge glaciers experienced a negative mass balance, while mass balance of surge-type glaciers was heterogeneous (Table 3). Khurdopin Glacier experienced a positive mass balance of 0.23 ± 0.02 m w.e. a^{-1}. Conversely, Batura and Yazgil Glaciers experienced negative mass balance of −0.24 ± 0.02 m w.e. a^{-1} and −0.24 ± 0.02 m w.e. a^{-1}. Hispar Glacier, as the largest glacier in the Hunza Basin, experienced a stable mass balance of −0.02 ± 0.02 m w.e. a^{-1}.

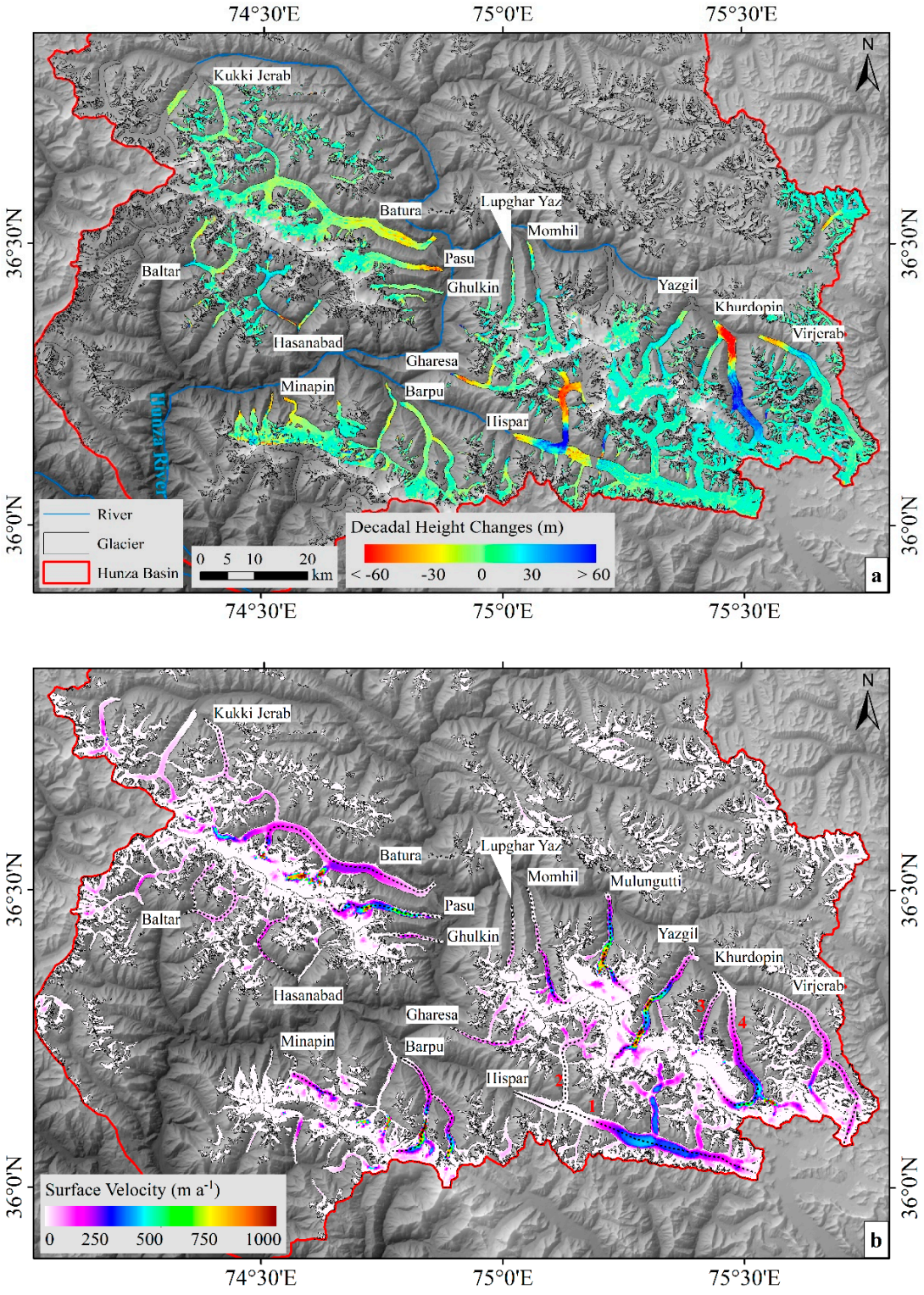

Figure 2. Glacier height changes and surface velocities for the Hunza Basin. (**a**) Surface elevation changes (ΔH) between 2000 and 2014 are based on SRTM and TerraSAR-X/TanDEM-X data. (**b**) Glacier surface velocities in 2014. The black dashed lines indicate the centerlines of each glacier. Numbers indicate different branches of specific glaciers (1: the main branch of Hispar; 2: the north branch of Hispar; 3: the west branch of Khurdopin; 4: the east branch of Khurdopin).

Table 3. Mean surface elevation changes and mass balance for the single glaciers and different regions in the Hunza Basin for the period 2000–2014. Glacier area are acquired from the Randolph Glacier Inventory 6.0. Mean ΔH is mean surface elevation change and mass balance is the annual mass budgets.

Region/Glacier Name	Glacier Area (km^2)	Mean ΔH (m)	Mass Balance (m w.e. a^{-1})
Kukki Jerab	41.1	−1.58 ± 0.07	−0.12 ± 0.02
Batura *	311.4	−3.14 ± 0.07	−0.24 ± 0.02
Pasu	62.1	−1.98± 0.07	−0.14 ± 0.02
Ghulkin	30.5	−3.75 ± 0.07	−0.27 ± 0.02
Lupghar Yaz	16.9	−1.58± 0.07	−0.11± 0.02
Momhil	73.2	1.81 ± 0.07	0.13 ± 0.02
Yazgil *	133.7	3.44 ± 0.07	0.24 ± 0.02
Khurdopin *	203.2	3.27 ± 0.07	0.23 ± 0.02
Virjerab *	167.3	1.20 ± 0.07	0.08 ± 0.02
Hispar *	495.3	−0.27 ± 0.07	−0.02 ± 0.02
Gharesa *	77.9	−2.19 ± 0.07	−0.16 ± 0.02
Barpu	105.0	−2.64± 0.07	−0.19± 0.02
Minapin	56.0	−3.88 ± 0.07	−0.27 ± 0.02
Hasanabad *	87.9	1.23 ± 0.07	0.09 ± 0.02
Baltar	91.1	−0.92 ± 0.07	−0.07 ± 0.02
Surge glaciers	1623.9	−0.78 ± 0.07	0.06 ± 0.02
Non-surge glaciers	1254.3	−0.40 ± 0.07	−0.03 ± 0.02
Debris-covered region	514.0	−5.39 ± 0.07	−0.38 ± 0.02
Clean-ice region	2364.2	0.05 ± 0.07	0.01 ± 0.02
Below 5100 m a.s.l.	1342.7	−3.01 ± 0.07	−0.21 ± 0.02
Above 5100 m a.s.l.	1535.0	1.50 ± 0.07	0.11 ± 0.02
Total	2878.2	−0.61 ± 0.07	−0.04 ± 0.02

* Surge-type glaciers.

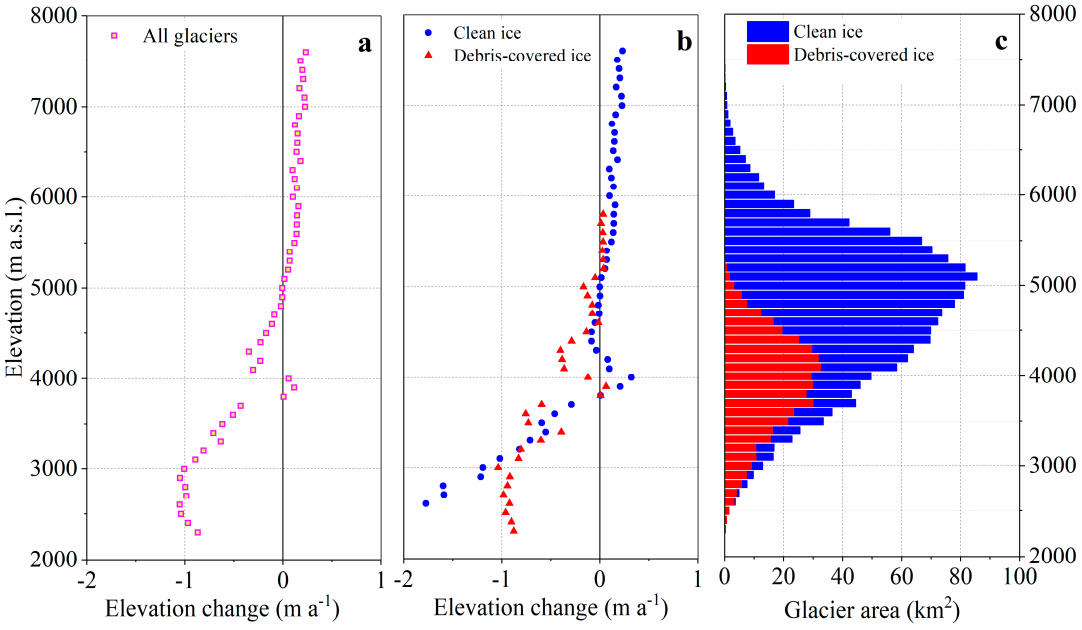

Figure 3. Glacier elevation changes and glacier area distribution at each 100 m interval by altitude in the Hunza Basin for the period 2000–2014. (**a**) Elevation changes for all glaciers. (**b**) Elevation changes for clean ice and debris-covered ice. (**c**) Distribution of 2014 glacier area.

4.2. Surface Velocity

Through visual inspection of the successive satellite imagery and examining the spatiotemporal evolution of surface velocities of each glacier, 16 glaciers in the Hunza Basin were classified into surge

and non-surge types. Their characteristics, including area, debris cover, elevation, and the length of centerline, are listed in Table 4.

Table 4. Attributes of the glaciers in this study. All attributes are acquired from the Randolph Glacier Inventory 6.0.

Glacier Name	Area (km^2)	Debris Cover (%)	Max/Min Elevation (m)	Median Elevation (m)	Max Length (km)	Mean Slope (Degree)	Mean Aspect (Degree)
Non-surging							
Kukki Jerab	41.1	39.1	6828/3597	4769	19.994	24.3	0
Pasu	62.1	2.9	7487/2578	5095	23.651	24.4	74
Ghulkin	30.5	17.9	7295/2556	5364	17.099	29.1	70
Lupghar Yaz	16.9	35.1	7157/3446	5175	15.288	25.9	360
Momhil	73.2	19.1	7506/2881	5630	30.252	29.3	7
Mulungutti	97.7	5.9	7799/2911	5664	23.889	26.9	8
Barpu	105.0	15.8	7432/2810	5093	29.588	22.3	4
Minapin	56.0	8.2	7178/2541	4346	18.834	26.7	359
Baltar	91.1	25.9	7688/3005	4898	20.516	31.2	246
Surging							
Batura *	311.4	22.2	7725/2595	4932	59.662	25	63
Yazgil *	133.7	6.2	7709/3234	5910	31.403	24.4	34
Khurdopin *	203.2	16.0	7718/3314	5391	31.640	23.6	21
Virjerab *	167.3	16.3	6368/3592	5241	40.178	23.1	11
Hispar *	495.3	28.0	7794/3110	4854	54.453	23.3	252
Gharesa *	77.9	13.4	7523/3825	5542	21.541	28.7	241
Hasanabad *	87.9	17.7	7737/2626	5084	21.070	32.2	164

* Surge-type glaciers.

Nine glaciers, having shown no significant change in surface features, were classified as non-surge glaciers in this study. Comparing the velocity profiles, there had no significant fluctuation in surface velocities of non-surge glaciers during 1990–2018 (Figure 4). For Kukki Jerab Glacier, a significant increase of surface velocity was observed along the profile, until a maximum of ~70 m a^{-1} was reached approximately 11 km from the terminus. While the maximum velocity of Barpu Glacier was ~1200 m a^{-1} between 14 km and 15 km from the terminus. Among all non-surge glaciers, only Minapin Glacier experienced a slight deceleration during 2001–2018 compared to 1990–2000. In the middle parts of Minapin (6–11 km from the terminus), the average surface velocity was ~160 m a^{-1} before 2000 and then decreased to ~125 m a^{-1} after 2000.

Seven glaciers were identified as surge-type glaciers, with 22 discrete surge events during the investigated period (Table 5). All surge-type glaciers experienced surge events more than once over the study period.

For Hasanabad, Virjerab, and Hispar Glaciers, we captured surge events twice in each glacier during 1990–2018 (Figure 5). Profiles of Hasanabad revealed two surge events between 8 km and 14 km from the terminus—the first from 1995–1997, and the second from 2014–2016. The interval of the surge events is ~17 years, which can be regarded as the surge cycle period of Hasanabad. The two surge events of Virjerab occurred in the same position (7–27 km from the terminus), with ~11 years interval. The first surge event lasted ~4 years from 2004–2007, and the second surge event began from 2018; it could be a beginning of a long-term surge event. While the two surge events of Hispar occurred in different position, the first surge event occurred in the north branch (4–9 km from the terminus) between 2009 and 2011, and the second surge event occurred in the main branch (20–44 km from the terminus) between 2014 and 2016 (Figure 6).

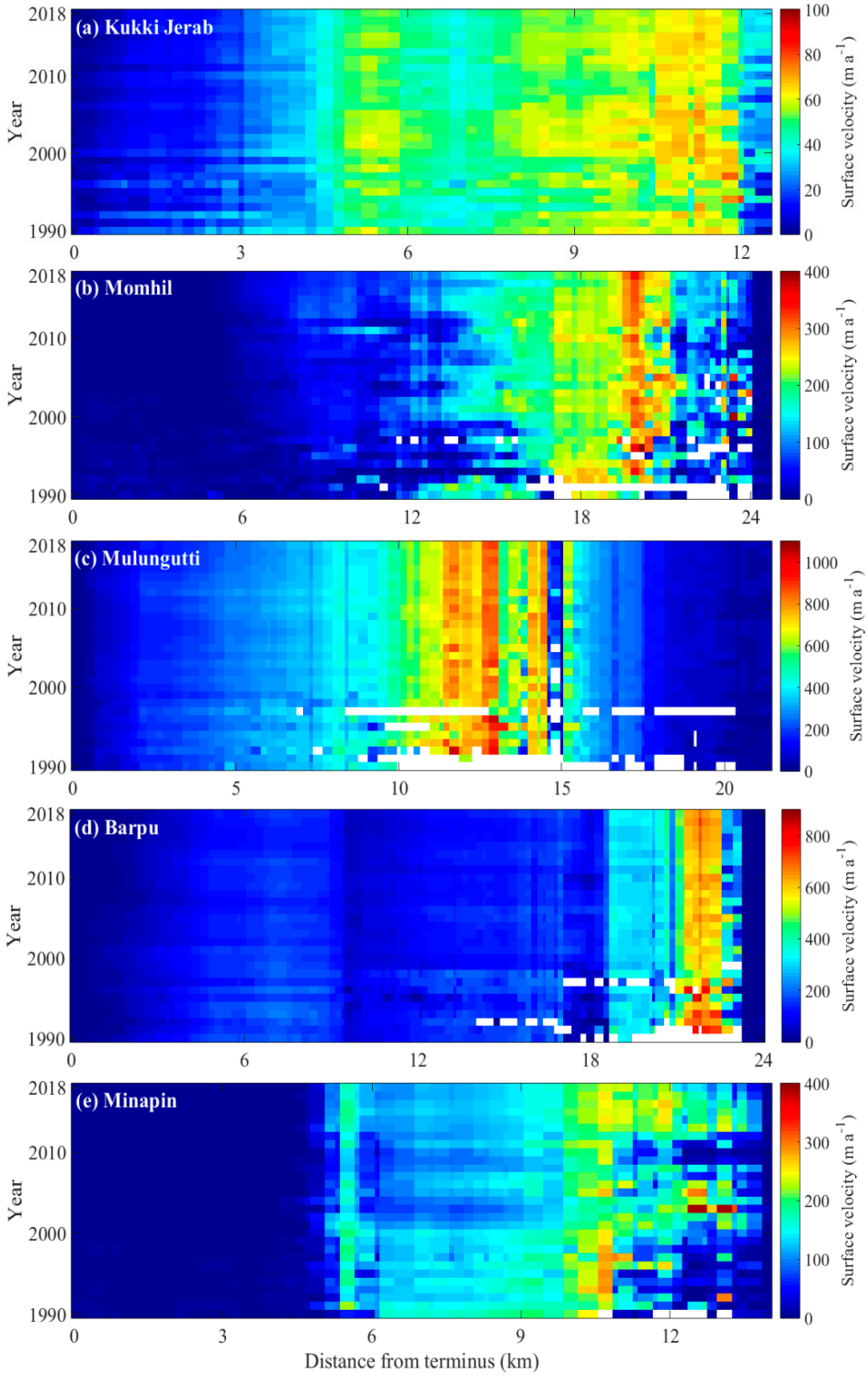

Figure 4. Evolution of annual surface velocities of non-surge glaciers along the longitudinal profiles (see Figure 2b). (**a**) Kukki Jerab Glacier. (**b**) Momhil Glacier. (**c**) Mulungutti Glacier. (**d**) Barpu Glacier. (**e**) Minapin Glaicer.

Table 5. Detailed information of each surge glacier in this study including evidence of each surge event, the initiating and terminating year, and surge duration.

Glacier Name	Evidence of Surge Events	Surge Initiating Year	Surge Terminating Year	Surge Duration
Batura	Clear acceleration and deceleration in velocity profiles; surface features show clear movement.	1990 2005 2013	1995 2010 2018	5 5 5
Yazgil	Clear acceleration and deceleration in velocity profiles; surface features show clear movement; looped moraines; terminus advanced during 1997–1998.	1997 2005 2010 2018	1998 2006 2011	2 2 2
Khurdopin (east branch)	Clear acceleration and deceleration in velocity profiles; surface features show clear movement; looped moraines; disappearance of glacial ponds.	1998 2016	1999 2018	2 3
Khurdopin (west branch)	Clear acceleration and deceleration in velocity profiles; looped moraines.	1990 1998 2008 2017	1992 2000 2010 2018	3 3 3 2
Virjerab	Clear acceleration and deceleration in velocity profiles; surface features show clear movement.	2004 2018	2007	4
Hispar (main branch)	Clear acceleration and deceleration in velocity profiles; surface features show clear movement; disappearance of glacial ponds.	2014	2016	3
Hispar (north branch)	Clear acceleration and deceleration in velocity profiles; surface features show clear movement; a clear surge front in satellite image.	2009	2011	3
Gharesa	Clear acceleration and deceleration in velocity profiles.	1995 2001 2015	1997 2003 2015	3 3 1
Hasanabad	Clear acceleration and deceleration in velocity profiles.	1995 2014	1997 2016	3 3

Three surge events were captured in Batura and Gharesa Glaciers during 1990–2018 (Figure 5). Profiles of Batura revealed that the three surge events all lasted ~6 years in the periods of 1990–1995, 2005–2010 and 2013–2018, respectively (Figure 6). The three surge events of Gharesa lasted ~3 years in the periods of 1995–1997, 2001–2003, and 2015–2017, respectively. The significant difference of two glaciers is the peak velocities of surge events—the average peak velocity of surge events was ~200 m a^{-1} in Batura, while it was ~100 m a^{-1} in Gharesa. This could be the main reason for the different durations of surge events. Meanwhile, the peak velocities of three surge events decreased gradually from 1990–2018, with 230, 200, and 170 m a^{-1} in Batura and 110, 100, and 90 m a^{-1} in Gharesa, respectively.

For Yazgil Glacier, four surge events were captured during 1990–2018 (Figure 5). From the terminus to accumulation area, there have two peak velocities in profiles of Yazgil (13–15 km and 19–22 km from the terminus). The first peak velocity was induced by the increase of slope, and there were no significant fluctuation in surface velocities above the altitude of first peak velocity over the study period. Below the altitude of first peak velocity, profiles of Yazgil revealed four surge events between 2 km and 11 km from the terminus, with 1997–1998, 2005–2006, 2010–2011, and 2018, respectively. These surge events lasted ~2 years, and the peak velocities of surge events decreased gradually from 1990–2018.

Profiles of the two branches of Khurdopin Glacier revealed that two surge events occurred in the east branch, and four surge events occurred in the west branch (Figure 5). In the east branch of Khurdopin, the two surge events lasted ~3 years in the periods of 1998–2000 and 2016–2018 (Figure 6). The interval of the surge events is ~16 years, if it be taken as a surge cycle period, the east branch of Khurdopin could be about to enter a long-term quiescent phase. The four surge events in the west branch lasted ~2 years, with ~7 years interval. The latest surge event began in 2018; this indicated that the west branch is entering a short-term active surge phase.

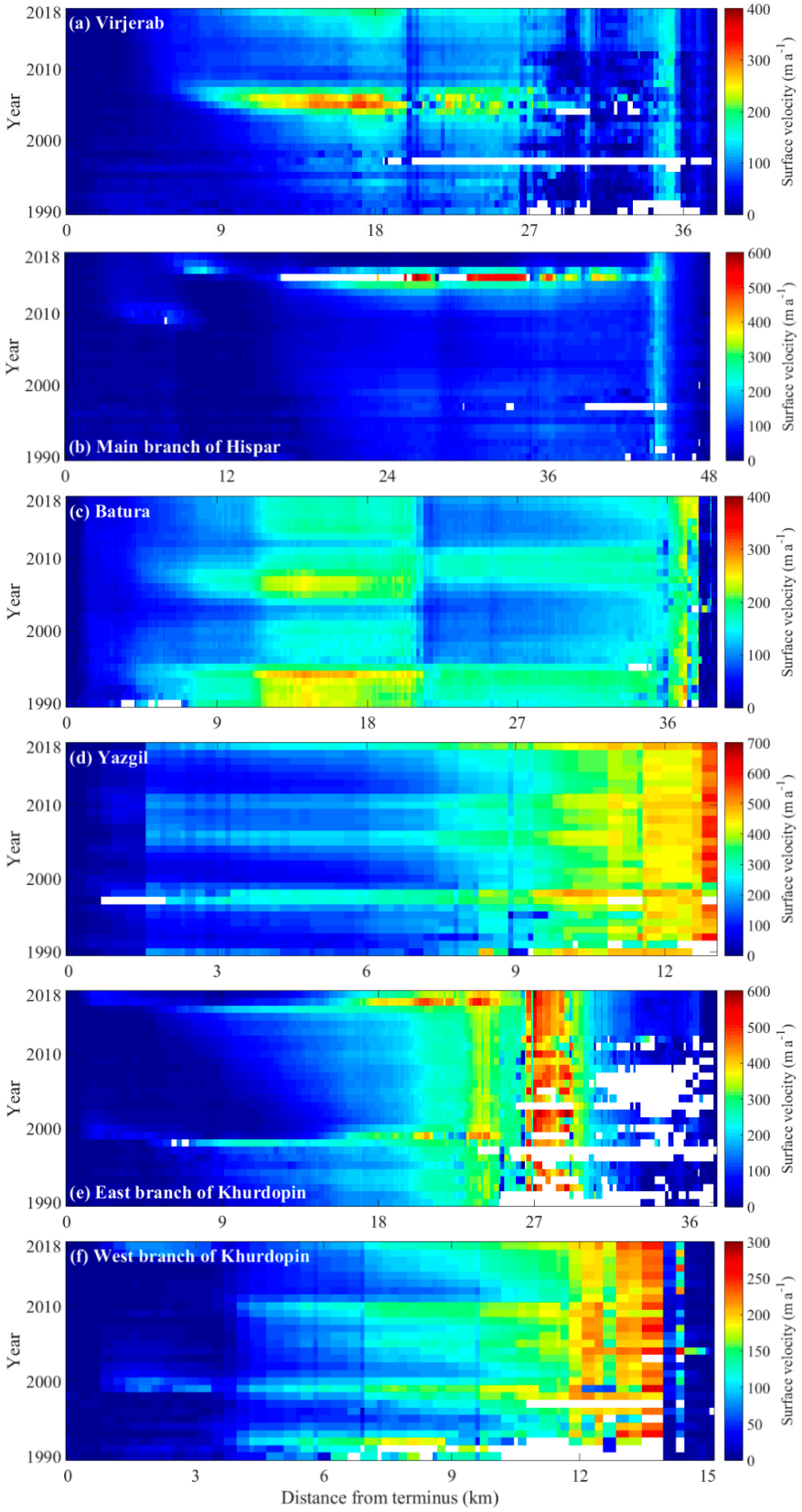

Figure 5. Evolution of annual surface velocities of surge glaciers along the longitudinal profiles (see Figure 2b) showing the spatial extent of the surges and how they evolved in time. (**a**) Virjerab. (**b**) Main branch of Hispar. (**c**) Batura. (**d**) Yazgil. (**e**) East branch of Khurdopin. (**f**) West branch of Khurdopin.

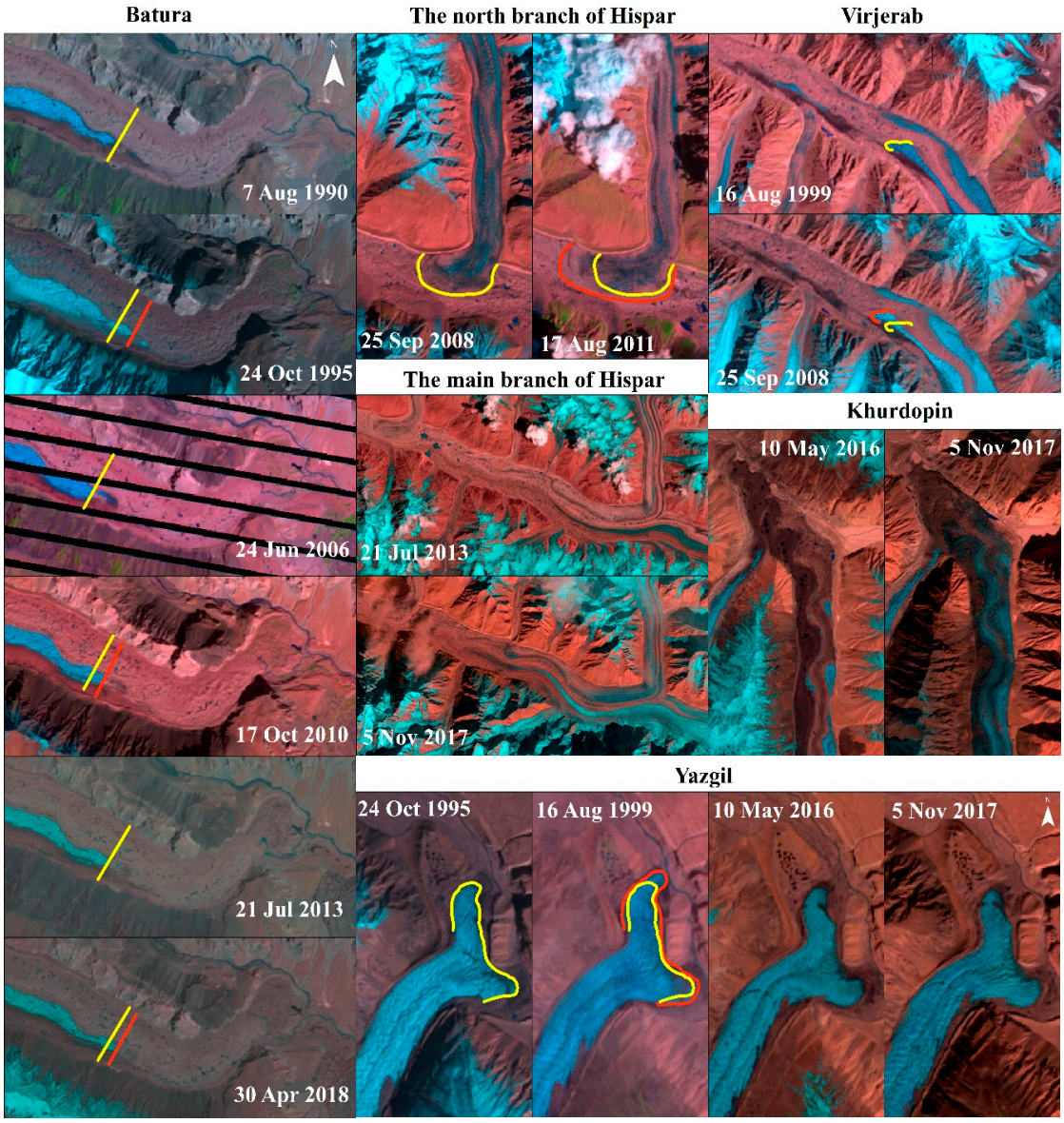

Figure 6. Comparison of the surge glaciers before and after surge events. The yellow lines show the positions of visible surface features in the earlier images and the red lines show the positions of the same surface features in recent images.

5. Discussion

5.1. Glacier Mass Balance

Previous studies revealed both negative and positive glacier mass balances in the study area. Gardelle et al. [9] showed a slight mass gain of +0.09 ± 0.18 m w.e. a^{-1} using the geodetic method based on C-band SRTM and SPOT5 DEMs between 2000 and 2008. However, Kääb et al. [30] and Gardner et al. [3] observed slight mass loss in the Karakoram, with glacier mass changes of −0.06 ± 0.04 m and −0.10 ± 0.14 m w.e. a^{-1} derived from SRTM and ICESat altimetry measurements during 2003–2009, respectively. Lin et al. [46] recorded a near-stable mass balance of −0.020 ± 0.064 m w.e. a^{-1} during 2000–2014 in the western Karakoram. Brun et al. [8] presented a mean mass loss of −0.03 ± 0.14 m w.e. a^{-1} from 2000–2016 in Karakoram. In this study, a slight mass loss of −0.04 ± 0.02 m w.e. a^{-1} was measured in the Hunza Basin. Compared to previous studies, the result of Gardelle et al. [9] were slightly different than those of other studies. Given that large uncertainty existed in previous studies, it is concluded that glaciers in west Karakoram experienced a near-stable mass balance since 2000.

In the Hunza Basin, debris cover has an accelerating effect on surface melting overall, while it plays different roles in different elevation ranges, with insulating and accelerating effects below and above 3500 m a.s.l., respectively. Except for debris cover, supraglacial/proglacial lakes and ice cliffs may also affect surface melting (Figure 7). Many crevasses and supraglacial lakes were developed in the ablation area, and the surface meltwater and liquid precipitation can flow down into the glaciers by crevasses. The englacial melt funnels/holes collapsed due to the coexistence of thick debris and inner ablation, and then ice cliffs and supraglacial lakes formed easily. The very fine debris attached to ice cliff, can reduce the ice albedo and absorb more shortwave radiations [56]. Hence, because of the effect of heat conduction, supraglacial lakes and ice cliffs aggravated the glacier surface melting.

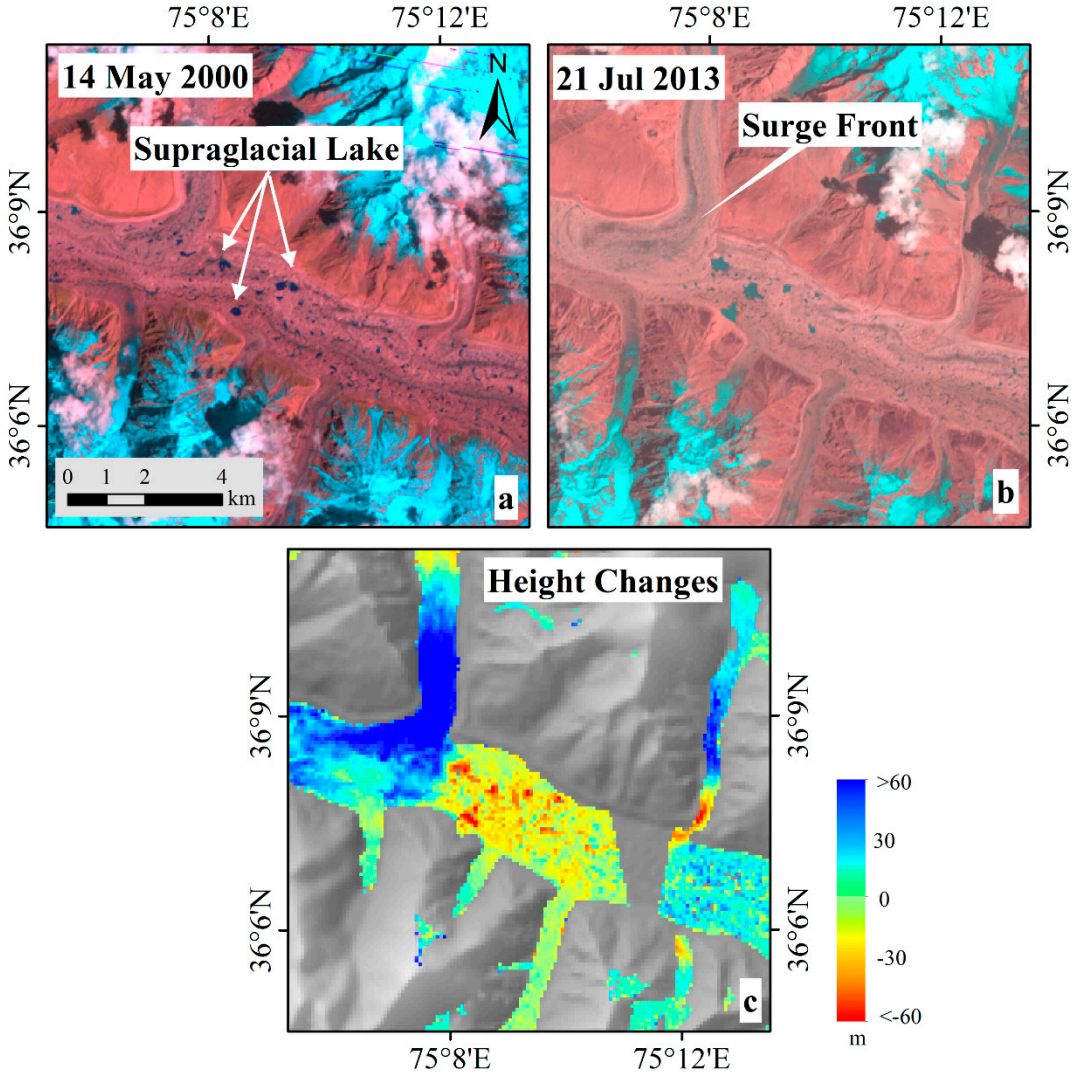

Figure 7. Landsat images (**a**,**b**) and surface height changes (**c**) in the main branch of Hispar. Images (**a**,**b**) were acquired on 14 May 2000 and 21 July 2013, respectively.

For surge glaciers, large volumes of ice were stored at high elevation for many decades before rapidly discharging the mass down-glacier during surge events. In short time scales, the surface elevation of the ablation area thickened significantly. A significant thickening was observed in the 3800–4100 m, which was the main reason for this is glacier surging in the north branch of Hispar between 2009–2011 (Figure 7). However, that ice came from high elevation and experienced a significant thinning at low elevation over long time scales. Therefore, surge-type glaciers in the Hunza Basin experienced a greater mass loss than non-surge-type glaciers. It is concluded that even though some

surge-type glaciers may have fluctuations in mass balance over short-time scales, their inclusion will not have a significant influence on overall mass balance in regional assessments.

5.2. Glacier Surface Velocity

Previous studies have shown that glacier surges, controlled by hydrology, tend to decelerate during summer and accelerate during winter [57,58]. This indicated that a seasonal signal could be exist to hydrologically controlled surge front propagation, whereas thermally controlled glacier surges can initiate at any time because these surges rely on the conditions of the glacier bed. Although there is no enough data to analyze the thermal regime of surge events, cold-based ice is considered to predominate at lower and higher elevations, thick warm-based ice predominates at middle elevations [14], and this has been borne out in Aru Glacier [5]. Meanwhile, profiles of several surge glaciers (Batura, the east branch of Khurdopin, Virjerab) revealed that surface velocities accelerated gradually before surging (Figure 5). This phenomenon meets the characteristic of thermally controlled surges. In order to detect if there has been a seasonal signal in surge events, seasonal variabilities of surface velocities were estimated from Landsat imageries with a high temporal resolution (Figure 8). The duration of glacier surges in the Hunza Basin is commonly 2–3 years and no more than ~5 year. The surge of the main branch of Hispar lasted more than one year, initiated in December 2014 and terminated in June 2016. Except for this surge event, surface velocities of Hispar did not significantly fluctuate during June 2013–March 2019 (Figure 9a). This suggests that these flow instabilities in Hispar can be attributed to a thermally controlled surge. However, surge events in Yazgil and the west branch of Khurdopin are similar to the surge event of Kelayayilake Glacier in Pamir, which was initiated in winter and terminated in the following summer [6]. It is reported that water discharge reduced significantly before and during the surge; therefore, the surge event of Kelayayilake can be regarded as a hydrologically controlled surge. Even though there have no hydrological data in the Hunza Basin to analyze the processes of water discharge, profiles of Yazgil revealed that surface velocities have a significant seasonal fluctuation during 2013–2019 (Figure 9b). Apparently, surge events of Yazgil are partially hydrologically controlled.

Except for the thermal and hydrological conditions, the geomorphological characteristics of glaciers, such as surface features, the size of the accumulation area, the width of the outlet, an surface slope, have a significant impact on glacier surge [5,7,20,54]. Seven surge glaciers with 22 surge events were identified in the Hunza Basin over the study period, and all surge events occurred in the middle parts of glaciers. Due to the obstruction of debris cover and long glacier tongues, surging ice were inhibited to reach the terminus; therefore, the termini of these glaciers remained stable after the surging [54]. New crevasses appeared, surface features, i.e., ice cliffs and supraglacial lakes, were rearranged, and the remnant of a previous glacier surge was overridden; all of these resulted from the spatial difference of surface velocities [7,54]. In turn, ice cliffs and supraglacial lakes aggravate the surface melting and more meltwater flowed down into glacier via crevasses. Then, sufficient hydrological conditions can prompt glacier surge. Besides, the main branch of Hispar has a broad outlet, which make ice transport to downstream stable, resulting in a longer surge cycle period. While Yazgil Glacier has a narrow outlet and a large accumulation area, ice/snow accumulates quickly and is frequently transported downstream, resulting in a shorter surge cycle period. Although cycle periods of glacier surge vary widely between individual glaciers, in general, the narrower the outlet and the larger of the accumulation area, the shorter of the surge cycle period [54].

According to the surge cycle period during 1990–2018, some glaciers are about to enter a quiescent phase, whereas some glaciers will enter an active phase. The first surge event of Virjerab lasted ~4 years from 2004–2007, and the second surge event began in 2018. The characteristics of profiles of surface velocities at the same position in the years before a surge were similar to each other, which indicated that it is approaching its next surge. For Hispar, Batura, and Khurdopin, longer surge cycle periods resulted from a broad outlet or a glacier surge having just terminated so that there has not much ice that could be transported downstream. This indicates that those glaciers are about to enter a quiescent

phase. As mentioned above, flow instabilities can be attributed to thermal and hydrological control and the geomorphological characteristics of different individuals. These factors are influenced by climate change. In the context of global warming, the thermal and hydrological conditions change accordingly. For example, four surge events were captured in Yazgil during 1990–2018; with a relatively shorter surge cycle period, surges will occur more frequently in the future according to the cycle period. However, the peak velocities of surge events in Yazgil decreased gradually from 1990 to 2018. Due to atmospheric warming, Yazgil experienced a significant mass loss during 2000–2014; this could weaken the thermal and hydrological conditions, resulting in a gradual decrease of the peak velocities of surge events.

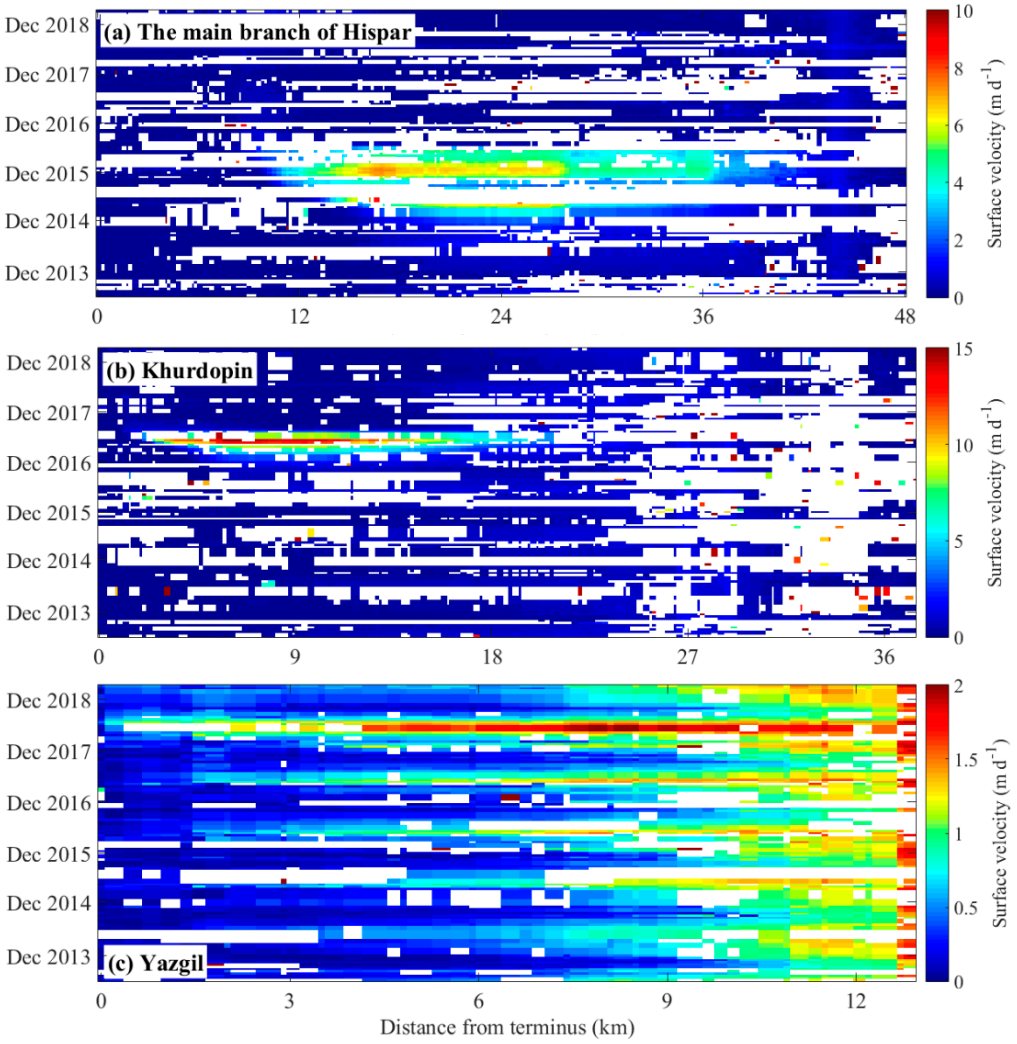

Figure 8. Evolution of seasonal surface velocities of Hispar, Khurdopin, and Yazgil Glaciers along the longitudinal profiles (see Figure 2b).

Although some other surge glaciers remain undiscovered, and such surge-type glaciers in the Hunza Basin represent a small part of all glaciers in HMA, the investigation of fast glacier flow, glacier surge and processes have a great contribution to glacier research [59]. Many surge events, rapid acceleration and deceleration, and decreased peak velocities of surge events give us a new insight into the "Karakoram anomaly" in the context of glacier mass loss in HMA.

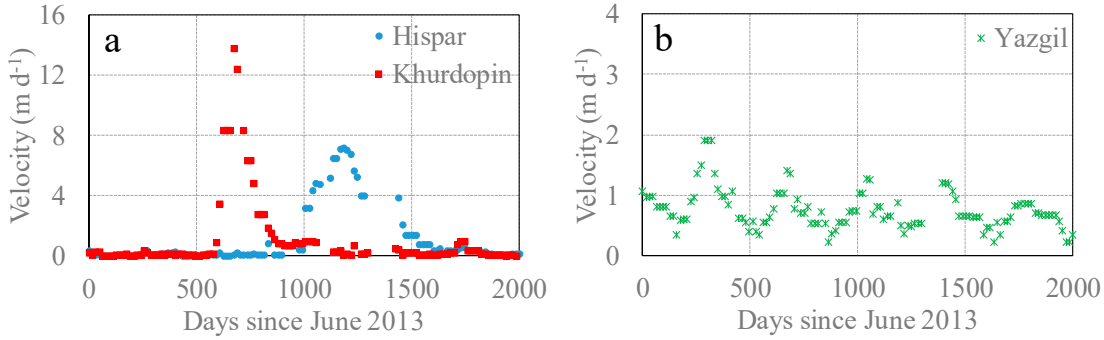

Figure 9. Temporal evolution of surge velocity for (**a**) Hispar, Khurdopin, and (**b**) Yazgil Glaciers. The surge durations of Hispar and Khurdopin are both more than 300 days, and a significant seasonal signal exists in Yazgil.

5.3. The Relationship between Mass Balance and Surface Velocity

All the non-surge-type glaciers in the Hunza Basin experienced a negative mass balance during 2000–2014. Except for Minapin Glacier, there have been no significant fluctuation in surface velocities of non-surge glaciers over three decades. Negative mass balance weakens the thermal condition but produces more meltwater, which can flow down into glaciers via crevasses and moulins and enhance the hydrological conditions. Therefore, glacier mass loss would not result in the decrease of surface velocity significantly over short time scales. For surge glaciers, there has been a rapid acceleration and deceleration in surface velocities, while mass balance was heterogeneous over the study period. Overall, mass balance increased with altitude, and glaciers experienced a significant thinning in the 2700–5100 m a.s.l. range due to the accelerating effect of debris cover, while it turned to mass gain above 5100 m a.s.l. during 2000–2014. This can cause an increase of the glacier gradient, resulting in an increase of driving stresses and ice velocities [60,61].

Our data indicated that even though some surge-type glaciers may have fluctuations in mass balance over short time scales, their inclusion will not have a significant influence on overall mass balance in regional assessments. Glaciers experienced a mass gain above 5100 m a.s.l., and then more ice was transported from up-glacier to terminus due to the rapid acceleration. Mass loss at higher elevation resulted from glacier surge; meanwhile, climate warming caused a quick mass loss at lower elevation. This suggests that glacier surge could result in a greater mass loss compared to non-surge-type glaciers over long time scales [8,9,21].

5.4. Climatic Considerations

The Hunza Basin climate is characterized by the westerlies, and the glaciers have experienced a near-stable mass balance since 2000. Previous studies indicate that this balanced pattern of mass balance is related to the changes in precipitation [9]. The Global Precipitation Climatology Project (GPCP) data set shows precipitation increasing over the Pamir and the Karakoram since 1970 [2]. In addition, the mean summer temperature in the Karakoram has been decreasing since 1961 [62]. These precipitation increases in winter and temperature decreases in summer result in greater accumulation and reduced ablation. Due to the effect of glacier surging, large volumes of ice rapidly discharged the mass down-glacier during surge events and experienced a significant thinning at low elevation over long time scales. Therefore, a nearly balanced glacier mass budget was present in the Hunza Basin.

In order to analyze the relationship between glacier surge and extreme precipitation, Climatic Research Unit TS V4.03 (CRU V4.03) data was employed in this study. The CRU V4.03 data is the gridded time-series dataset from 1901 to 2018 [63], which was constructed using the Climate Anomaly Method with observations of the whole world. The dataset provides monthly total precipitation with a spatial resolution of 0.5°×0.5°. The change of winter precipitation derived from this data is

shown in Figure 10. It is clear that winter precipitation increased slightly in the Hunza Basin during 1991–2018. This could provide an abundance of matter sources sufficient power for glacier surging. In addition, heavy precipitation in winter occurred in 1998, 2005, 2009, 2013, and 2017; meanwhile, several glacier surge events were initiated in the same year. Furthermore, heavy precipitation has become more frequent in recent decade, and these changes are consistent with the more frequent glacier surges. The IPCC AR5 suggests that the occurrence of heavy precipitation events might increase in the future [64], and this might induce more frequent glacier surges.

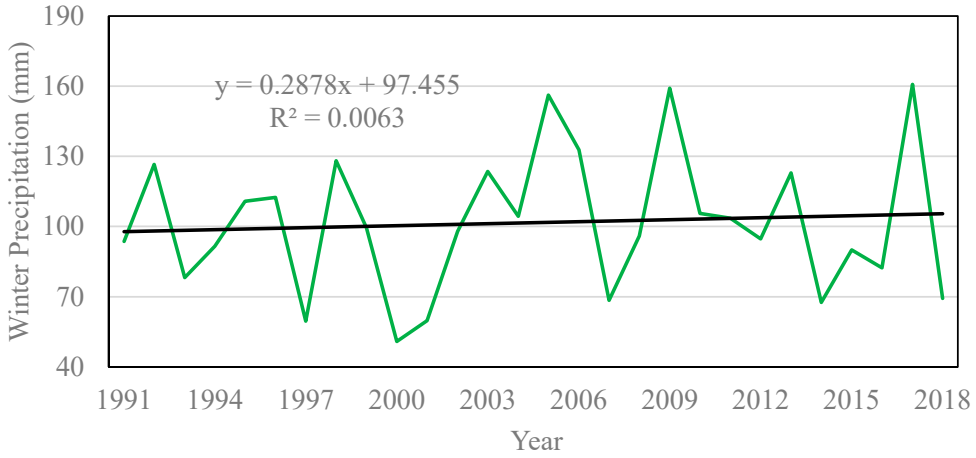

Figure 10. The change of winter precipitation in the Hunza Basin during 1991–2018.

6. Conclusions

In this study, the differential synthetic aperture radar interferometry (DInSAR) method on the SRTM DEM and TerraSAR-X/TanDEM-X were employed to calculate glacier mass balance in the Hunza Basin of the western Karakoram. The temporal and spatial evolution of glacial motion in the Hunza Basin were acquired from published data sets and Landsat images.

Glaciers in the Hunza Basin experienced a slight negative mass balance during 2000–2014. The debris cover has an acceleration effect on surface melting overall, whereas the debris cover has different impacts at different elevation ranges. Even though some surge-type glaciers may have fluctuations in mass balance over short time scales, their inclusion will not have a significant influence on overall mass balance in regional assessments over long time scales.

By analyzing and quantifying glacial motion from 1990 to 2018, seven glaciers were identified as surge-type glaciers in the Hunza Basin, with 22 discrete surge events from the studied glaciers. Flow instabilities can be attributed to thermal and hydrological control and the geomorphological characteristics of different individuals.

Author Contributions: Data curation and Original draft preparation, K.W.; Reviewing and Editing, S.L.; Data processing of Glacier Mass Balance, Z.J.; Data processing of Glacier Outlines, Y.Z.; Data processing of Debris Cover, F.X.; Data processing of Glacier Velocity, Y.G.; Data processing of Climate change, Y.Y.; Data processing of Glacier surging, A.A.T. and S.M. All authors have read and agreed to the published version of the manuscript.

Funding: This research was funded by the Fundamental Programme of the National Natural Science Foundation of China (grant no. 41801031; 41761144075), a grant of the Second Tibetan Plateau Scientific Expedition and Research Program (STEP, 2019QZKK0208), a project of the State Key Laboratory of Cryospheric Science (grant no. SKLCS-OP-2019-07), and a grant for talent introduction of Yunnan University (YJRC3201702).

Acknowledgments: The Landsat images and SRTM C-band data can be freely downloaded from http://glovis.usgs.gov (last access: 10 September 2018). We thank the USGS for free access to Landsat and SRTM C-band data. Randolph Glacier Inventory is available from GLIMS (https://www.glims.org/). All SAR processing was done with the GAMMA SAR and interferometric processing software. ITS_LIVE and GoLIVE are available from the Jet Propulsion Laboratory, NASA (https://its-live.jpl.nasa.gov/) and the National Snow & Ice Data Center (https://nsidc.org/). CRU TS V4.03 are available from the University of East Anglia (http://www.cru.uea.ac.uk/).

Conflicts of Interest: The authors declare no conflict of interest.

References

1. Immerzeel, W.W.; Lutz, A.F.; Andrade, M.; Bahl, A.; Biemans, H.; Bolch, T.; Hyde, S.; Brumby, S.; Davies, B.J.; Elmore, A.C.; et al. Importance and vulnerability of the world's water towers. *Nature* **2020**, *577*, 364–369. [CrossRef] [PubMed]
2. Yao, T.; Thompson, L.; Yang, W.; Yu, W.; Gao, Y.; Guo, X.; Yang, X.; Duan, K.; Zhao, H.; Xu, B.; et al. Different glacier status with atmospheric circulations in Tibetan Plateau and surroundings. *Nat. Clim. Chang.* **2012**, *2*, 663–667. [CrossRef]
3. Gardner, A.; Moholdt, G.; Cogley, J.G.; Wouters, B.; Arendt, A.; Wahr, J.; Berthier, E.; Hock, R.; Pfeffer, W.T.; Kaser, G.; et al. A reconciled estimate of glacier contributions to sea level rise: 2003 to 2009. *Science* **2013**, *340*, 852–857. [CrossRef] [PubMed]
4. Herreid, S.; Pellicciotti, F. The state of rock debris covering Earth's glaciers. *Nat. Geosci.* **2020**, *13*, 621–627. [CrossRef]
5. Kääb, A.; Leinss, S.; Gilbert, A.; Bühler, Y.; Gascoin, S.; Evans, S.G.; Bartelt, P.; Berthier, E.; Brun, F.; Chao, W.-A.; et al. Massive collapse of two glaciers in western Tibet in 2016 after surge-like instability. *Nat. Geosci.* **2018**, *11*, 114–120. [CrossRef]
6. Shangguan, D.; Liu, S.; Ding, Y.; Guo, W.; Xu, B.; Xu, J.; Jiang, Z. Characterizing the May 2015 Karayaylak Glacier surge in the eastern Pamir Plateau using remote sensing. *J. Glaciol.* **2016**, *62*, 944–953. [CrossRef]
7. Zhang, Z.; Liu, S.; Zhang, Y.; Wei, J.; Jiang, Z.; Kunpeng, W.U. Glacier variations at Aru Co in western Tibet from 1971 to 2016 derived from remote-sensing data. *J. Glaciol.* **2018**, *64*, 397–406. [CrossRef]
8. Brun, F.; Berthier, E.; Wagnon, P.; Kaab, A.; Treichler, D. A spatially resolved estimate of High Mountain Asia glacier mass balances, 2000–2016. *Nat. Geosci.* **2017**, *10*, 668–673. [CrossRef]
9. Gardelle, J.; Berthier, E.; Arnaud, Y.; Kaab, A. Region-wide glacier mass balances over the Pamir-Karakoram-Himalaya during 1999–2011. *Cryosphere* **2013**, *7*, 1885–1886. [CrossRef]
10. Zhou, Y.; Li, Z.; Li, J.; Zhao, R.; Ding, X. Glacier mass balance in the Qinghai–Tibet Plateau and its surroundings from the mid-1970s to 2000 based on Hexagon KH-9 and SRTM DEMs. *Remote Sens. Environ.* **2018**, *210*, 96–112. [CrossRef]
11. Scherler, D.; Bookhagen, B.; Strecker, M.R. Spatially variable response of Himalayan glaciers to climate change affected by debris cover. *Nat. Geosci.* **2011**, *4*, 156–159. [CrossRef]
12. Wu, K.; Liu, S.; Jiang, Z.; Xu, J.; Wei, J.; Guo, W. Recent glacier mass balance and area changes in the Kangri Karpo Mountains from DEMs and glacier inventories. *Cryosphere* **2018**, *12*, 103–121. [CrossRef]
13. Gardelle, J.; Berthier, E.; Arnaud, Y. Slight mass gain of Karakoram glaciers in the early twenty-first century. *Nat. Geosci.* **2012**, *5*, 322–325. [CrossRef]
14. Quincey, D.J.; Braun, M.; Glasser, N.F.; Bishop, M.P.; Hewitt, K.; Luckman, A. Karakoram glacier surge dynamics. *Geophys. Res. Lett.* **2011**, *38*, 113–120. [CrossRef]
15. Rowan, A.V.; Egholm, D.L.; Quincey, D.J.; Glasser, N.F. Modelling the feedbacks between mass balance, ice flow and debris transport to predict the response to climate change of debris-covered glaciers in the Himalaya. *Earth Planet. Sci. Lett.* **2015**, *430*, 427–438. [CrossRef]
16. Cuffey, K.M.; Paterson, W.S.B. *The Physics of Glaciers*, 4th ed.; Butterworth-Heinemann: Burlington, MA, USA; Elsevier: Oxford, UK, 2010.
17. Paul, F.; Bolch, T.; Kääb, A.; Nägler, T.; Nuth, C.; Scharrer, K.; Shepherd, A.; Strozzi, T.; Ticconi, F.; Bhambri, R.; et al. The glaciers climate change initiative: Methods for creating glacier area, elevation change and velocity products. *Remote Sens. Environ.* **2015**, *162*, 408–426. [CrossRef]
18. Dehecq, A.; Gourmelen, N.; Gardner, A.; Brun, F.; Goldberg, D.; Nienow, P.W.; Berthier, E.; Vincent, C.; Wagnon, P.; Trouve, E. Twenty-first century glacier slowdown driven by mass loss in High Mountain Asia. *Nat. Geosci.* **2019**, *12*, 22–27. [CrossRef]
19. Dehecq, A.; Gourmelen, N.; Trouve, E. Deriving large-scale glacier velocities from a complete satellite archive: Application to the Pamir–Karakoram–Himalaya. *Remote Sens. Environ.* **2015**, *162*, 55–66. [CrossRef]
20. Quincey, D.J.; Glasser, N.F.; Cook, S.J.; Luckman, A. Heterogeneity in Karakoram glacier surges. *J. Geophys. Res. Earth Surf.* **2015**, *120*, 1288–1300. [CrossRef]
21. Rankl, M.; Kienholz, C.; Braun, M. Glacier changes in the Karakoram region mapped by multimission satellite imagery. *Cryosphere* **2014**, *8*, 977–989. [CrossRef]
22. Farinotti, D.; Immerzeel, W.W.; de Kok, R.J.; Quincey, D.J.; Dehecq, A. Manifestations and mechanisms of the Karakoram glacier Anomaly. *Nat. Geosci.* **2020**, *13*, 8–16. [CrossRef] [PubMed]

23. Goudie, A. The geomorphology of the Hunza valley, Karakoram mountains, Pakistan. *Int. Karakoram Proj.* **1984**, *2*, 359–410.
24. Qureshi, M.A.; Yi, C.L.; Xu, X.K.; Li, Y.K. Glacier status during the period 1973–2014 in the Hunza Basin, Western Karakoram. *Quat. Int.* **2017**, *444*, 125–136. [CrossRef]
25. Immerzeel, W.W.; Pellicciotti, F.; Shrestha, A.B. Glaciers as a proxy to quantify the spatial distribution of precipitation in the Hunza basin. *Mt. Res. Dev.* **2012**, *32*, 30–39. [CrossRef]
26. Young, G.; Hewitt, K. Hydrology research in the upper Indus basin, Karakoram Himalaya, Pakistan. *IAHS Publ.* **1990**, *190*, 139–152.
27. Bookhagen, B.; Burbank, D.W. Toward a complete Himalayan hydrological budget: Spatiotemporal distribution of snowmelt and rainfall and their impact on river discharge. *J. Geophys. Res. Earth Surf.* **2010**, *115*, F03019. [CrossRef]
28. Tahir, A.A.; Chevallier, P.; Arnaud, Y.; Ahmad, B. Snow cover dynamics and hydrological regime of the Hunza River basin, Karakoram Range, Northern Pakistan. *Hydrol. Earth Syst. Sci.* **2011**, *15*, 2275–2290. [CrossRef]
29. Consortium, R. *Randolph Glacier Inventory—A Dataset of Global Glacier Outlines: Version 6.0: Technical Report*; Global Land Ice Measurements from Space: Boulder, CO, USA, 2017.
30. Kääb, A.; Berthier, E.; Nuth, C.; Gardelle, J.; Arnaud, Y. Contrasting patterns of early twenty-first-century glacier mass change in the Himalayas. *Nature* **2012**, *488*, 495. [CrossRef]
31. Hewitt, K. Tributary glacier surges: An exceptional concentration at Panmah Glacier, Karakoram Himalaya. *J. Glaciol.* **2007**, *53*, 181–188. [CrossRef]
32. Rashid, I.; Abdullah, T.; Glasser, N.F.; Naz, H.; Romshoo, S.A. Surge of Hispar Glacier, Pakistan, between 2013 and 2017 detected from remote sensing observations. *Geomorphology* **2018**, *303*, 410–416. [CrossRef]
33. Shah, A.; Ali, K.; Nizami, S.M.; Jan, I.U.; Hussain, I.; Begum, F. Risk assessment of Shishper Glacier, Hassanabad Hunza, North Pakistan. *J. Himal. Earth Sci.* **2019**, *52*, 1–11.
34. Scherler, D.; Wulf, H.; Gorelick, N. Global Assessment of Supraglacial Debris-Cover Extents. *Geophys. Res. Lett.* **2018**, *45*, 11798–11805. [CrossRef]
35. Housman, I.; Chastain, R.; Finco, M. An Evaluation of Forest Health Insect and Disease Survey Data and Satellite-Based Remote Sensing Forest Change Detection Methods: Case Studies in the United States. *Remote Sens.* **2018**, *10*, 1184. [CrossRef]
36. Dozier, J. Spectral signature of alpine snow cover from the Landsat Thematic Mapper. *Remote Sens. Environ.* **1989**, *28*, 9–22. [CrossRef]
37. Wu, K.-P.; Liu, S.-Y.; Guo, W.-Q.; Wei, J.-F.; Xu, J.-L.; Bao, W.-J.; Yao, X.-J. Glacier change in the western Nyainqentanglha Range, Tibetan Plateau using historical maps and Landsat imagery: 1970–2014. *J. Mt. Sci.* **2016**, *13*, 1358–1374. [CrossRef]
38. Paul, F.; Bolch, T.; Briggs, K.; Kääb, A.; McMillan, M.; McNabb, R.W.; Nagler, T.; Nuth, C.; Rastner, P.; Strozzi, T.; et al. Error sources and guidelines for quality assessment of glacier area, elevation change, and velocity products derived from satellite data in the Glaciers_cci project. *Remote Sens. Environ.* **2017**, *203*, 256–275. [CrossRef]
39. Guo, W.-Q.; Liu, S.-Y.; Xu, J.; Wu, L.; Shangguan, D.; Yao, X.; Wei, J.; Bao, W.; Yu, P.; Liu, Q.; et al. The second Chinese glacier inventory: Data, methods and results. *J. Glaciol.* **2015**, *61*, 357–372. [CrossRef]
40. Krieger, G.; Moreira, A.; Fiedler, H.; Hajnsek, I. TanDEM-X: A Satellite Formation for High-Resolution SAR Interferometry. *IEEE Trans. Geosci. Remote Sens.* **2007**, *45*, 3317–3341. [CrossRef]
41. Li, G.; Lin, H.; Ye, Q. Heterogeneous decadal glacier downwasting at the Mt. Everest (Qomolangma) from 2000 to~ 2012 based on multi-baseline bistatic SAR interferometry. *Remote Sens. Environ.* **2018**, *206*, 336–349. [CrossRef]
42. Neckel, N.; Braun, A.; Kropáček, J.; Hochschild, V. Recent mass balance of the Purogangri Ice Cap, central Tibetan Plateau, by means of differential X-band SAR interferometry. *Cryosphere* **2013**, *7*, 1623–1633. [CrossRef]
43. Wu, K.; Liu, S.; Jiang, Z.; Xu, J.; Wei, J. Glacier mass balance over the central Nyainqentanglha Range during recent decades derived from remote-sensing data. *J. Glaciol.* **2019**, *65*, 422–439. [CrossRef]
44. Melanie, R.; Matthias, B. Glacier elevation and mass changes over the central Karakoram region estimated from TanDEM-X and SRTM/X-SAR digital elevation models. *Ann. Glaciol.* **2016**, *51*, 273–281.
45. Goldstein, R.M.; Werner, C.L. Radar interferogram filtering for geophysical applications. *Geophys. Res. Lett.* **1998**, *25*, 4035–4038. [CrossRef]

46. Lin, H.; Li, G.; Cuo, L.; Andrew, H.; Ye, Q. A decreasing glacier mass balance gradient from the edge of the Upper Tarim Basin to the Karakoram during 2000–2014. *Sci. Rep.* **2017**, *7*, 1–9. [CrossRef]
47. Neckel, N.; Loibl, D.; Rankl, M. Recent slowdown and thinning of debris-covered glaciers in south-eastern Tibet. *Earth Planet. Sci. Lett.* **2017**, *464*, 95–102. [CrossRef]
48. Rignot, E.; Echelmeyer, K.; Krabill, W. Penetration depth of interferometric synthetic-aperture radar signals in snow and ice. *Geophys. Res. Lett.* **2001**, *28*, 3501–3504. [CrossRef]
49. Huss, M. Density assumptions for converting geodetic glacier volume change to mass change. *Cryosphere* **2013**, *7*, 877–887. [CrossRef]
50. Gardner, A.S.; Fahnstock, M.; Scambos, T. *ITS_LIVE Regional Glacier and Ice Sheet Surface Velocities*; Data archived at National Snow and Ice Data Center, 2019. Available online: https://its-live.jpl.nasa.gov/ (accessed on 6 August 2020).
51. Gardner, A.S.; Moholdt, G.; Scambos, T.; Fahnstock, M.; Ligtenberg, S.; van den Broeke, M.; Nilsson, J. Increased West Antarctic and unchanged East Antarctic ice discharge over the last 7 years. *Cryosphere* **2018**, *12*, 521–547. [CrossRef]
52. Leprince, S.; Barbot, S.; Ayoub, F.; Avouac, J.-P. Automatic and Precise Orthorectification, Coregistration, and Subpixel Correlation of Satellite Images, Application to Ground Deformation Measurements. *IEEE Trans. Geosci. Remote Sens.* **2007**, *45*, 1529–1558. [CrossRef]
53. Heid, T.; Kääb, A. Repeat optical satellite images reveal widespread and long term decrease in land-terminating glacier speeds. *Cryosphere* **2012**, *6*, 467–478. [CrossRef]
54. Lv, M.; Guo, H.; Lu, X.; Liu, G.; Yan, S.; Ruan, Z.; Ding, Y.; Quincey, D.J. Characterizing the behaviour of surge-and non-surge-type glaciers in the Kingata Mountains, eastern Pamir, from 1999 to 2016. *Cryosphere* **2019**, *13*, 219–236. [CrossRef]
55. Scherler, D.; Leprince, S.; Strecker, M.R. Glacier-surface velocities in alpine terrain from optical satellite imagery—Accuracy improvement and quality assessment. *Remote Sens. Environ.* **2008**, *112*, 3806–3819. [CrossRef]
56. Reid, T.D.; Brock, B.W. Assessing ice-cliff backwasting and its contribution to total ablation of debris-covered Miage glacier, Mont Blanc massif, Italy. *J. Glaciol.* **2014**, *60*, 3–13. [CrossRef]
57. Björnsson, H. Hydrological characteristics of the drainage system beneath a surging glacier. *Nature* **1998**, *395*, 771. [CrossRef]
58. Raymond, C.F. How do glaciers surge? A review. *J. Geophys. Res. Solid Earth* **1987**, *92*, 9121–9134. [CrossRef]
59. Clarke, G.K.C. Fast glacier flow: Ice streams, surging, and tidewater glaciers. *J. Geophys. Res. Solid Earth* **1987**, *92*, 8835–8841. [CrossRef]
60. Benn, D.I.; Bolch, T.; Hands, K.; Gulley, J.; Luckman, A.; Nicholson, L.; Quincey, D.; Thompson, S.; Toumi, R.; Wiseman, S. Response of debris-covered glaciers in the Mount Everest region to recent warming, and implications for outburst flood hazards. *Earth Sci. Rev.* **2012**, *114*, 156–174. [CrossRef]
61. Quincey, D.J.; Luckman, A.; Benn, D. Quantification of Everest region glacier velocities between 1992 and 2002, using satellite radar interferometry and feature tracking. *J. Glaciol.* **2009**, *55*, 596–606. [CrossRef]
62. Fowler, H.; Archer, D. Conflicting signals of climatic change in the Upper Indus Basin. *J. Clim.* **2006**, *19*, 4276–4293. [CrossRef]
63. Harris, I.; Jones, P.D.; Osborn, T.J.; Lister, D.H. Updated high-resolution grids of monthly climatic observations—The CRU TS3.10 Dataset. *Int. J. Climatol.* **2014**, *34*, 623–642. [CrossRef]
64. IPCC. *Climate Change 2013: The Physical Science Basis. Contribution of Working Group I to the Fifth Assessment Report of the Intergovernmental Panel on Climate Change*; Cambridge University Press: Cambridge, UK; New York, NY, USA, 2013.